FINITE ELEMENT MODEL OF VIBRATING OVERHEAD CONDUCTORS WITH VARIABLE BENDING STIFFNESS

Sébastien LANGLOIS, Frédéric LÉVESQUE, Frédéric LÉGERON
Department of Civil Engineering, Université de Sherbrooke - 2500 Boul. de l'Université, Sherbrooke, Québec, J1K 2R1 - Canada
Sebastien.Langlois@USherbrooke.ca
Frederic.Levesque@USherbrooke.ca
Frederic.Legeron@USherbrooke.ca

Introduction

Aeolian vibrations may cause fretting fatigue failure at or near the location of clamped devices (suspension clamps, dampers, spacers, etc.). The mitigation of these vibrations is thus a necessity to improve transmission lines reliability and life expectation. The most common way to control these vibrations is to install dampers on conductors. There is a need to develop numerical design tools for transmission line dampers. Before even assessing the behaviour of a damper-conductor system, the mechanical behaviour of the conductor itself needs to be modelled with sufficient precision. Models to describe the non linear variation of bending stiffness of conductors have been proposed [1, 2]. In a companion paper, Paradis and Légeron [3] developed an alternative model. Dastous [4] implemented the behaviour law of Papailiou [2] in a finite element model for the study of low-tension substation conductors. Guérard et al [5, 6] made dynamic tests on a cable bench to study specifically bending stiffness of conductors and developed a linear finite element model. Variable bending stiffness has not yet been implemented in a dynamic model for the study of aeolian vibrations.

The objective of the present paper is to include variable bending stiffness in a time history finite element model. The deformed shape obtained is compared to the one measured during vibration tests on a short span (5.83 m) presented in a companion paper [7]. Three hypotheses for bending stiffness are studied: (i) linear bending stiffness equals to 50% of the theoretical maximum stiffness (EI_{max}); (ii) non linear bending stiffness according to Papailiou [2]; (iii) non linear bending stiffness according to Paradis and Legeron [3] (hereafter named Paradis model).

METHODOLOGY

The open source finite element software Code Aster [8] was used in this study. In order to modify the bending stiffness of the conductor while keeping constant the axial stiffness, Euler beam elements and large displacement cable elements were superimposed. To model variable stiffness, four to six non linear beam elements and one cable element are actually placed at each mesh subdivision.

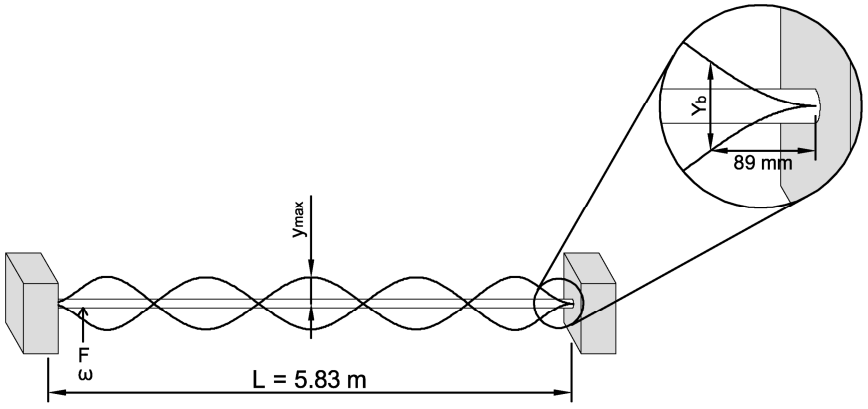

Figure 1: Sketch of the numerical model.

A sketch of the model is shown in figure 1. The model is excited at 0.33 m from the left end by a sinusoidal vertical force F with frequency ω corresponding to mode 3 of the cable. Displacements are recorded at the mid-span anti-node (y_{max}) and at five locations in the right-hand near field, including at 89 mm from the right end (bending amplitude Y_b). The model assumes that the translation and rotation at span ends is fully blocked in all directions.

The model has a total 130 mesh subdivisions: 20 subdivisions of 8.9 mm each in the left near field, 40 subdivisions of 8.9 mm in the right near field and 70 subdivisions of 75.7 mm in the free field. The mesh is hence more refined near supports, where curvature variations are more important. It was verified that further refinements in the near fields did not change the deformed shape. In order to predict the non linear response of the cable, a direct time integration method has been used. The integration scheme selected is Newmark-beta with β=0.25 and γ=0.5, therefore avoiding numerical damping. The damping ratio calculated from the experiments of Lévesque et al. [7] is included in the model through Rayleigh damping [9].

For models with linear bending stiffness, a time history of 12 seconds is calculated with a time step of 1E-03 second. The frequency calculated theoretically is preferred to the experimental frequency to ensure that the mode is well developed. The amplitude of the force, which is constant with time, is found iteratively such that the experimental anti-node 0-peak displacement (y_{max}) is within 2% of the experimental value at the end of the 12-seconds time history. For linear calculations, for which the computation time is around 20 minutes (without post-processing), the root-finding algorithm called 'secant method' is used to find the correct amplitude of force.

For models with non linear bending stiffness, a time history of 12 seconds is calculated with a time step of 1E-04 second. The excitation frequency f (in Hz) is calculated theoretically with the bending stiffness equal to the initial bending stiffness (zero curvature) of the corresponding behaviour law (see figure 2 for example). To help convergence, the amplitude of the force varies between zero and the maximum force during the first 10 seconds of the time history. The force amplitude is then constant for the last two seconds in order to avoid transient effects. Again, the maximum force applied is found iteratively such that the experimental anti-node amplitude is reached. Each run takes between 20 and 40 hours on an Intel Xeon 2.8 GHz computer.

To model non linear bending stiffness, an elastic-perfectly-plastic behaviour for beam elements is used. First of all, an elastic beam element with bending stiffness equal to the minimum stiffness according to the behaviour law is defined. Second, a small number of elastic-perfectly-plastic beams

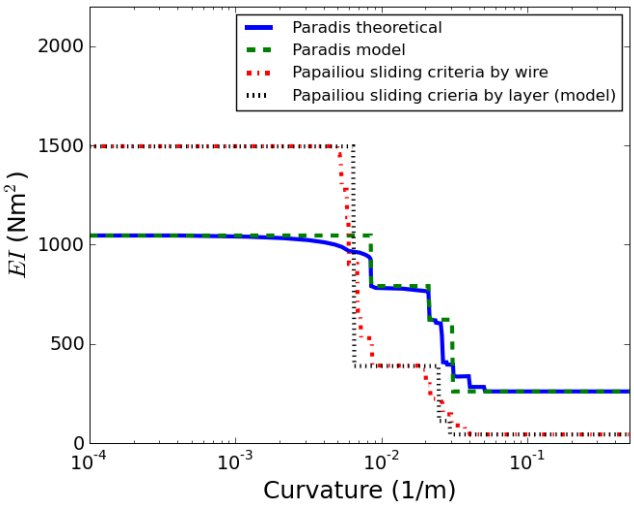

Figure 2: Variable bending stiffness laws for Drake at tension 15% RTS.

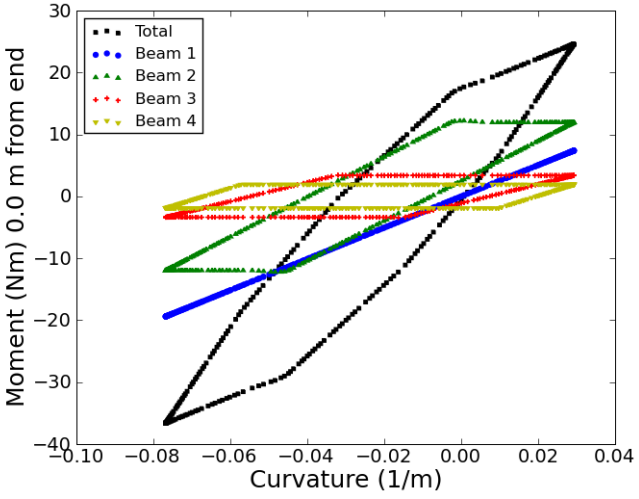

Figure 3: Example of moment-curvature relation split by beam for test with Paradis stiffness.

are superimposed to simulate the slippage of wires. Overall, the number of beams corresponds to the number of conductor layers. For Papailiou's model, the maximum bending stiffness of each elastic-plastic beam corresponds to the additional bending stiffness of a particular layer when it is in a sticking state as compared to the slipping state. For the model of Paradis, which has a slip criterion by wire rather than a slip criterion by layer, the parameters of each beam are adjusted such that the overall bending stiffness-curvature curve of the model best match the one of the theoretical behaviour law. Figure 2 shows the various relations between bending stiffness and curvature and Figure 3 shows the moment-curvature relation during a numerical test. The coefficient of friction considered in the calculation of variable bending stiffness is 0.5, as suggested by Papailiou [2].

RESULTS

Tables 1 to 3 show the comparison between the experimental deformed shape of the vibrating Drake conductor and the simulated deformed shape for three distinct hypotheses for bending stiffness. The last five columns show the normalised deformed shape with respect with the experimental deformed shape. Due to convergence problems, the numerical tests for Papailiou behaviour law were done for bending amplitudes Y_b=0.3mm and lower only.

Table 1: Deformed shape for Drake conductor at tension H=15% RTS.

Stiffness	f (Hz)	F (N)	Y_{45} (mm)	Y_b (mm)	Y_{178} (mm)	Y_{267} (mm)	y_{max} (mm)	Y/Y_{exp} 45 mm	Y/Y_{exp} 89 mm	Y/Y_{exp} 178 mm	Y/Y_{exp} 267 mm	y/y_{exp} ventre
Y_b=0.1mm												
Exp.	31.16	2.19	0.036	0.102	0.331	0.629	1.415	-	-	-	-	-
Papailiou	34.88	38.00	0.041	0.143	0.429	0.773	1.423	1.16	1.40	1.30	1.23	1.01
Paradis	33.51	5.50	0.025	0.092	0.314	0.614	1.443	0.70	0.90	0.95	0.98	1.02
$0.5EI_{max}$	32.54	4.00	0.026	0.095	0.327	0.637	1.409	0.73	0.93	0.99	1.01	1.00
Y_b=0.2mm												
Exp.	31.13	6.78	0.068	0.200	0.643	1.235	2.745	-	-	-	-	-
Papailiou	34.90	155.00	0.128	0.363	0.964	1.635	2.711	1.88	1.82	1.50	1.32	0.99
Paradis	33.53	19.50	0.052	0.188	0.635	1.223	2.729	0.76	0.94	0.99	0.99	0.99
$0.5EI_{max}$	32.55	7.30	0.050	0.186	0.637	1.238	2.742	0.74	0.93	0.99	1.00	1.00
Y_b=0.3mm												
Exp.	31.11	14.31	0.105	0.300	0.951	1.825	3.960	-	-	-	-	-
Papailiou	34.90	340.00	0.251	0.694	1.729	2.822	3.999	2.39	2.31	1.82	1.55	1.01
Paradis	33.53	66.00	0.095	0.321	1.016	1.900	4.000	0.90	1.07	1.07	1.04	1.01
$0.5EI_{max}$	32.56	18.35	0.072	0.266	0.913	1.774	3.934	0.68	0.89	0.96	0.97	0.99
Y_b=0.4mm												
Exp.	31.07	24.24	0.140	0.399	1.251	2.382	5.120	-	-	-	-	-
Paradis	33.53	119.00	0.139	0.472	1.438	2.623	5.143	0.99	1.18	1.15	1.10	1.00
$0.5EI_{max}$	32.56	42.40	0.093	0.344	1.179	2.291	5.088	0.67	0.86	0.94	0.96	0.99
Y_b=0.5mm												
Exp.	31.07	35.54	0.177	0.501	1.553	2.940	6.140	-	-	-	-	-
Paradis	33.56	162.50	0.176	0.604	1.822	3.281	6.169	0.99	1.21	1.17	1.12	1.00
$0.5EI_{max}$	32.59	76.30	0.111	0.411	1.408	2.734	6.078	0.63	0.82	0.91	0.93	0.99
Y_b=0.6mm												
Exp.	31.18	46.47	0.214	0.599	1.829	3.464	7.065	-	-	-	-	-
Paradis	33.64	195.00	0.208	0.718	2.165	3.872	7.110	0.97	1.20	1.18	1.12	1.01
$0.5EI_{max}$	32.67	121.50	0.129	0.477	1.634	3.170	7.046	0.61	0.80	0.89	0.92	1.00

Table 2: Deformed shape for Drake conductor at tension H=25% RTS.

Stiffness	f (Hz)	F (N)	Y_{45} (mm)	Y_b (mm)	Y_{178} (mm)	Y_{267} (mm)	y_{max} (mm)	Y/Y_{exp} 45 mm	Y/Y_{exp} 89 mm	Y/Y_{exp} 178 mm	Y/Y_{exp} 267 mm	y/y_{exp} ventre
Y_b=0.1mm												
Exp.	39.80	4.84	0.037	0.102	0.308	0.581	1.195	-	-	-	-	-
Papailiou	42.17	4.00	0.021	0.077	0.266	0.520	1.203	0.58	0.76	0.86	0.89	1.01
Paradis	41.22	2.85	0.023	0.083	0.284	0.550	1.204	0.62	0.81	0.92	0.95	1.01
$0.5EI_{max}$	40.15	8.93	0.026	0.093	0.310	0.588	1.173	0.70	0.91	1.01	1.01	0.98
Y_b=0.2mm												
Exp.	39.77	11.75	0.071	0.200	0.619	1.167	2.330	-	-	-	-	-
Papailiou	42.14	61.00	0.066	0.223	0.667	1.207	2.340	0.92	1.12	1.08	1.03	1.00
Paradis	41.18	14.00	0.048	0.173	0.575	1.099	2.351	0.68	0.87	0.93	0.94	1.01
$0.5EI_{max}$	40.12	14.70	0.052	0.187	0.624	1.183	2.364	0.73	0.94	1.01	1.01	1.01
Y_b=0.3mm												
Exp.	39.77	20.46	0.106	0.300	0.918	1.712	3.390	-	-	-	-	-
Papailiou	42.09	135.00	0.147	0.429	1.158	1.986	3.363	1.39	1.43	1.26	1.16	0.99
Paradis	41.13	30.00	0.074	0.266	0.878	1.658	3.435	0.70	0.89	0.96	0.97	1.01
$0.5EI_{max}$	40.06	17.30	0.074	0.270	0.900	1.706	3.413	0.70	0.90	0.98	1.00	1.01
Y_b=0.4mm												
Exp.	39.78	31.17	0.142	0.400	1.227	2.248	4.490	-	-	-	-	-
Paradis	41.19	80.00	0.119	0.398	1.247	2.302	4.557	0.84	1.00	1.02	1.02	1.01
$0.5EI_{max}$	40.12	21.30	0.099	0.359	1.194	2.264	4.528	0.70	0.90	0.97	1.01	1.01
Y_b=0.5mm												
Exp.	39.78	43.04	0.177	0.500	1.515	2.735	5.415	-	-	-	-	-
Paradis	41.23	120.00	0.152	0.500	1.518	2.763	5.304	0.86	1.00	1.00	1.01	0.98
$0.5EI_{max}$	40.16	32.80	0.119	0.430	1.432	2.713	5.431	0.67	0.86	0.95	0.99	1.00
Y_b=0.6mm												
Exp.	39.76	55.44	0.214	0.600	1.796	3.201	6.250	-	-	-	-	-
Paradis	41.27	151.00	0.194	0.635	1.885	3.383	6.284	0.90	1.06	1.05	1.06	1.01
$0.5EI_{max}$	40.20	55.44	0.137	0.498	1.657	3.138	6.287	0.64	0.83	0.92	0.98	1.01

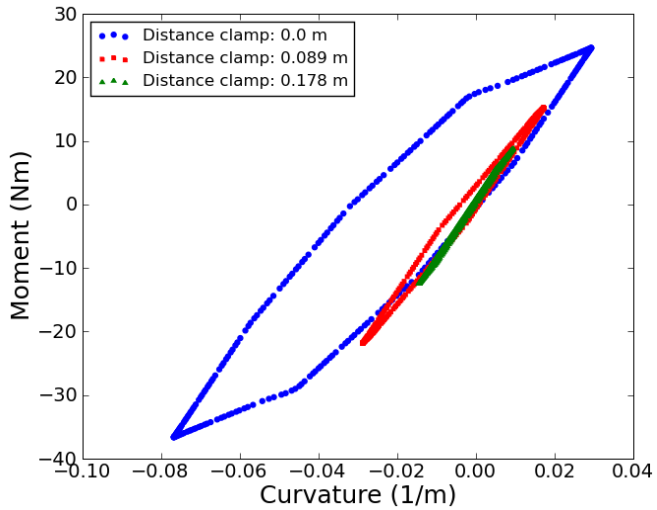

Figure 4: Example of moment-curvature relation for Paradis model.

Table 3: Deformed shape for Drake conductor at tension H=35% RTS.

Stiffness	f (Hz)	F (N)	Y_{45} (mm)	Y_b (mm)	Y_{178} (mm)	Y_{267} (mm)	y_{max} (mm)	Y/Y_{exp} 45 mm	Y/Y_{exp} 89 mm	Y/Y_{exp} 178 mm	Y/Y_{exp} 267 mm	y/y_{exp} ventre
Exp.	46.87	9.33	0.037	0.100	0.300	0.547	1.010	-	-	-	-	-
Papailiou	48.89	2.90	0.019	0.071	0.242	0.467	1.005	0.52	0.71	0.81	0.85	1.00
Paradis	48.13	2.70	0.021	0.077	0.259	0.493	1.010	0.57	0.77	0.86	0.90	1.00
$0.5EI_{max}$	47.06	13.80	0.025	0.090	0.291	0.540	1.002	0.68	0.90	0.97	0.99	0.99
Y_b=0.2mm												
Exp.	46.82	19.02	0.072	0.200	0.595	1.086	2.000	-	-	-	-	-
Papailiou	48.83	28.80	0.052	0.171	0.530	0.988	2.008	0.72	0.85	0.89	0.91	1.00
Paradis	48.08	6.80	0.042	0.151	0.505	0.962	1.971	0.58	0.76	0.85	0.89	0.99
$0.5EI_{max}$	47.01	28.40	0.049	0.175	0.569	1.056	1.960	0.68	0.88	0.96	0.97	0.98
Y_b=0.3mm												
Exp.	46.80	30.14	0.108	0.300	0.893	1.633	3.025	-	-	-	-	-
Papailiou	48.79	90.00	0.098	0.324	0.944	1.678	3.056	0.91	1.08	1.06	1.03	1.01
Paradis	48.04	20.00	0.070	0.248	0.805	1.510	3.010	0.65	0.83	0.90	0.92	1.00
$0.5EI_{max}$	46.97	34.37	0.075	0.267	0.868	1.612	2.996	0.69	0.89	0.97	0.99	0.99
Y_b=0.4mm												
Exp.	46.70	42.28	0.143	0.400	1.187	2.166	4.055	-	-	-	-	-
Paradis	47.71	34.00	0.096	0.343	1.108	2.066	4.064	0.67	0.86	0.93	0.95	1.00
$0.5EI_{max}$	46.64	34.35	0.099	0.354	1.151	2.141	3.994	0.69	0.89	0.97	0.99	0.99
Y_b=0.5mm												
Exp.	46.74	55.84	0.180	0.500	1.475	2.689	5.005	-	-	-	-	-
Paradis	47.89	53.00	0.125	0.442	1.417	2.627	5.084	0.70	0.88	0.96	0.98	1.02
$0.5EI_{max}$	46.82	37.85	0.124	0.443	1.437	2.670	4.975	0.69	0.89	0.97	0.99	0.99
Y_b=0.6mm												
Exp.	46.72	70.02	0.218	0.600	1.759	3.185	5.920	-	-	-	-	-
Paradis	47.92	78.00	0.157	0.535	1.679	3.080	5.852	0.72	0.89	0.95	0.97	0.99
$0.5EI_{max}$	46.85	40.76	0.146	0.522	1.693	3.143	5.856	0.67	0.87	0.96	0.99	0.99

Figure 4 shows the total moment-curvature obtained at various locations along the span. This type of graph allows defining the level and extent of sliding predicted by variable stiffness models. The dissection of the Drake specimens in Lévesque et al. [7] showed that sliding was observed up to 160 mm from the clamp. By comparison, the numerical tests with the model of Paradis showed some sliding up to 230 mm from the clamp.

ANALYSIS

Excitation Force

Because the modelled system is very sensitive, it was not possible to obtain the wanted level of vibration by simply applying the experimental excitation force and frequency. Having theoretically calculated the frequency, the force is then found with an iterative process. It is interesting to analyze how different the final force is from the experimental force. The excitation force required for each numerical test is found in Tables 1 to 3. For tests with $0.5EI_{max}$, the force is generally similar to the experimental value. For the non linear models, it is expected that the force is higher than the experimental force because the non linearity creates a hysteresis that dissipates energy. This adds to

the energy dissipation caused by the Rayleigh damping which is calculated to be equal to the total energy dissipation in the experiment. The fact that the force required for the tests with Papailiou's law is much higher than the experimental force indicates that the model of Papailiou overestimates the area within the hysteresis. This, in turn, indicates that the bending stiffness variation during vibration cycles is overestimated with the model of Papailiou. The model of Paradis, in which the bending stiffness never reaches the maximum and minimum theoretical values, hence appears to be more realistic.

Deformed Shape

As shown in figure 5, the peak-to-peak displacement at 45 mm and 89 mm from the clamp is smaller than the experimental displacement when assuming a constant bending stiffness of $0.5EI_{max}$. The normalised displacement near the clamp generally decreases with increasing level of vibration. This last phenomenon is less important for higher conductor tension. These observations are in agreement with the theoretical behaviour of cables when considering variable bending stiffness.

In figure 6, a comparison between the deformed shapes at 15% RTS for the two variable bending stiffness models is made. This graph clearly shows that the model of Paradis is more adequate to predict the deformed shape of vibrating conductors than the model of Papailiou. When looking at tables 2 and 3, it appears that the model of Papailiou gives on average adequate predictions for higher tensions. However, the dispersion of results is overall very large for this model when compared to the model of Paradis. Papailiou's behaviour law generally overestimates the variation of bending stiffness in vibrating conductors.

Figure 7 shows how the deformed shape near the clamp evolves with increasing level of vibration for the numerical tests with Paradis bending stiffness. For large amplitudes of vibration, the displacements at 89, 133, 178 and 267 mm are overestimated. Hence, even if the variation of bending stiffness is less important for the model of Paradis than for the model of Papailiou, it is still too sensitive to curvature variation. In summary, when comparing with the results of figure 5, it appears that whereas the model of Paradis allows predicting correctly the trends of bending stiffness variation, the results are not more accurate than using a constant bending stiffness of $0.5EI_{max}$. The displacements for $0.5EI_{max}$ are close to the values predicted by the Paradis model for low curvature. The statistics for the bending amplitude Y_b at 89 mm from the clamp are shown in Table 4.

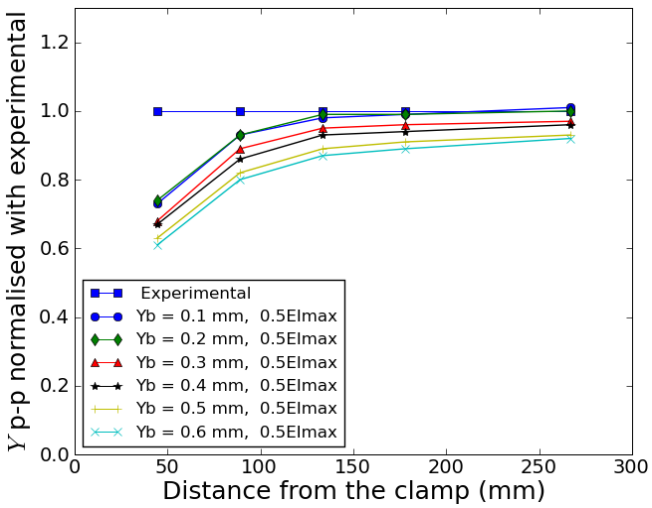

Figure 5: Normalised deformed shape with bending stiffness $0.5EI_{max}$.

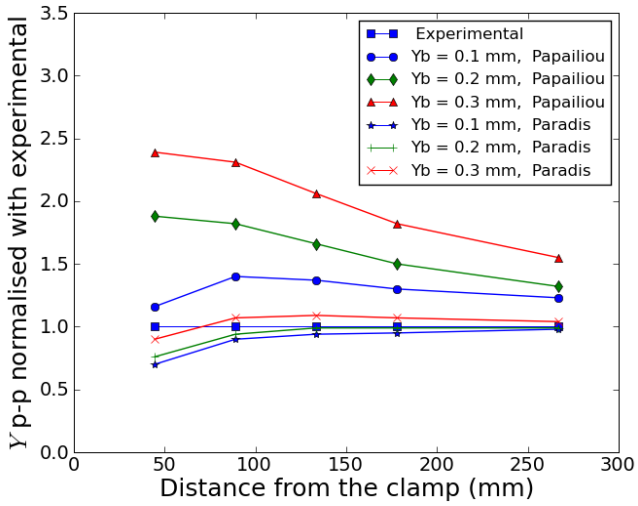

Figure 6: Comparison of deformed shape with bending stiffness Papailiou and Paradis.

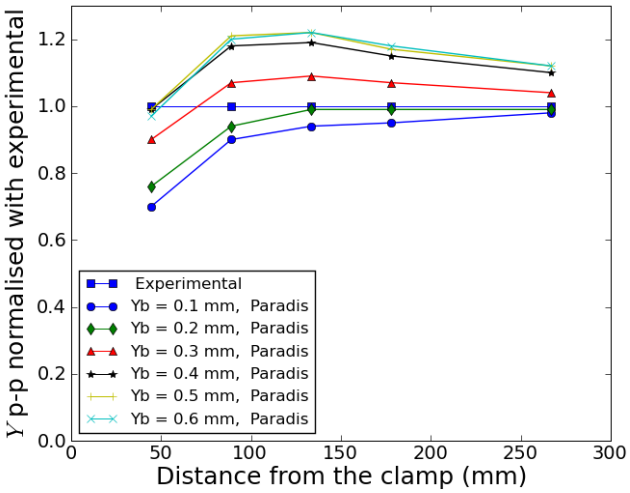

Figure 7: Normalised deformed shape with bending stiffness Paradis.

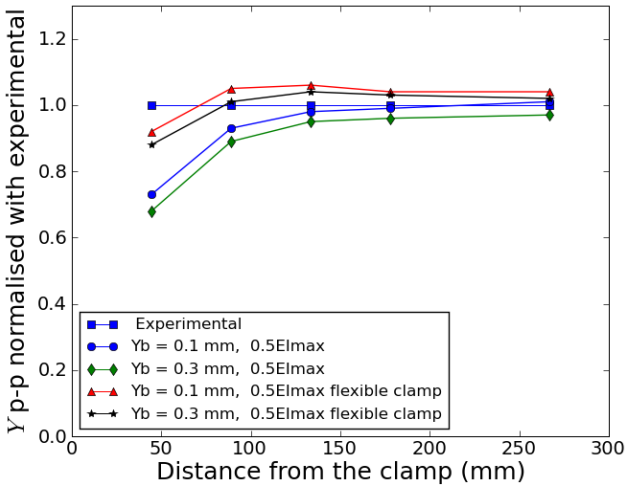

Figure 8: Normalised deformed shape with and without rotational flexibility at the clamp.

Table 4: Statistics for normalised displacements at 89 mm from the clamp.

Model	Mean	Standard deviation
Papailiou	1.28	0.53
Paradis	0.95	0.14
$0.5EI_{max}$	0.88	0.04

Another observation that can be drawn from figures 5 and 7 is that the displacement at 45 mm for low amplitude of vibration is always smaller than the experimental displacement. It seems that this apparent reduction of bending stiffness very close to the clamp is not linked to curvature variation and therefore cannot be predicted by theoretical bending stiffness models. As discussed in Lévesque et al. [7], many hypotheses could be raised to explain this phenomenon. In any case, the model could be adjusted to take into account these boundary conditions effects. In figure 8, two of the constant stiffness numerical tests were repeated but with a rotational spring at the clamp with stiffness value equals to 1.15E05 Nm^2. This value of stiffness is arbitrary but was applied to both tests to ensure that the flexibility at the clamp is a characteristic of the system. These two tests show results much closer to the experimental values.

CONCLUSIONS

In this paper, variable bending stiffness models were implemented in a dynamic finite element model for the study of the deformed shape of vibrating conductors. The following conclusions can be drawn from this study:

- The model of Paradis shows less dispersion in the prediction of conductor deformed shape than the model of Papailiou.
- The model of Paradis correctly predicts the trends of bending stiffness variation but is not more accurate than a constant bending stiffness of $0.5EI_{max}$.
- The variation of bending stiffness is in general less important than what is predicted by both non linear models.
- Some of the apparent bending stiffness variation observed experimentally may be due to boundary conditions effects and is independent of curvature variation.

Additional validation in both static and dynamic regimes would be required to successfully integrate theoretical bending stiffness models in the study of aeolian vibrations. The effect of boundary

conditions on the deformed shape of conductors near the clamp would need to be studied for both rigid and standard transmission line clamps, as well as new types of clamps.

Overall, it appears that using constant bending stiffness is adequate for modeling the deformed shape of vibrating conductors. This assumption may however be inaccurate for other applications such as the study of the kinematics in the near field for the determination of contact stresses involved with fretting fatigue. For such applications, it would be interesting to continue the work on theoretical bending stiffness models of cables and most importantly, to validate the models experimentally.

ACKNOWLEDGEMENTS

The financial support of Helix Uniformé and the guidance from Jean-Philippe Houle-Paradis are acknowledged. The project was realized within the private Research Chair HQT/RTE on Mechanics and Structures of Transmission Lines. The financial support of NSERC, Hydro-Québec TransÉnergie (HQT) and RTE is also acknowledged. Computational resources were provided by Calcul Québec and Compute Canada.

REFERENCES

[1] EPRI, 2009, *Transmission line reference book: Wind-induced conductor motion*, Electrical Power Research Institute, Palo Alto, CA, USA.

[2] K.O. Papailiou, 1997, "On the bending stiffness of transmission line conductors", *IEEE Trans. Power Del.*, vol. 12, issue 4, 1576-1588.

[3] J.-P. H. Paradis, F. Légeron, 2011, "Modeling of the free bending behaviour of a multilayer cable taking into account the tangential compliance of contact interfaces.", *Ninth International Symposium on Cable Dynamics*, Shanghai.

[4] J.-B. Dastous, 2005, "Nonlinear finite-element analysis of stranded conductors with variable bending stiffness using the tangent stiffness method", *IEEE Trans. Power Del.*, vol. 20, issue 1, 328-338.

[5] S. Guérard, P. Van Dyke, J.L. Lilien, 2009, "Evaluation of power line cable fatigue parameters based on measurements on a laboratory cable test span", *Eighth International Symposium on Cable Dynamics*, Paris.

[6] S. Guérard, J.L. Lilien, P. Van Dyke, 2009, "Vibrations of a short span, comparison between modelization and measurements performed on a laboratory span ", *Eighth International Symposium on Cable Dynamics*, Paris.

[7] F. Lévesque, S. Goudreau, S. Langlois, F. Légeron, 2011, "Experimental study of dynamic bending stiffness of overhead conductors", *Ninth International Symposium on Cable Dynamics*, Shanghai.

[8] EDF, Code Aster, http://www.code-aster.org, 2011.

[9] R.D. Cook, D.S. Malkus, M.E. Plesha, R.J. Witt, 2002, *Concepts and Applications of Finite Element Analysis,* 4rd ed., John Wiley, New York.